Indian Journal of Engineering & Materials Sciences
Vol. 32, February 2025, pp. 158-172
DOI: 10.56042/ijems.v32i01.2131

Use of gamma coated wire to optimize the WEDM process parameters for Nitronic-30

Nilesh Tanaji Mohite[a] & Geetanjali Vijay Patil[b*]
B.L.D.E.A's V.P. Dr. P.G. Halakatti College of Engineering and Technology, Vijaypur 586 101 India

Received: 31 May 2023; accepted 11 October 2024

Due to the complicated and non-linear behaviour, efficient and economical application of Wire Electrical Discharge Machining (WEDM) method is a challenge for the cutting-edge manufacturing period. The goal of the current study is to determine the best combination of input process parameters to achieve optimum material removal rate (MRR) and surface roughness (SR). Nitronic-30 is an austenitic stainless steel that has a high strength and good corrosion-resistant qualities. It has a wide range of possible uses in solid handling equipment, aqueous applications, and automotive components. Therefore, multi-objective optimization of Nitronic-30 on WEDM is necessary. RSM based Box Behnken design of experiments have been conducted using machining factors such as pulse on time (Ton), pulse off time (Toff), peak current (IP), and servo voltage (SV). Gamma coated wire have been used as electrode material for present analysis. This is the distinguishing factor of the current research. Surface roughness and material removal rate are two response variables that have been evaluated using Minitab-17 software. The process parameters proposed by Grey Relational Analysis (GRA) are Ton 115 (MU), Toff 50 (MU), IP 150 (A) and SV 60 (V) for obtaining optimal response variables as 2.07 µm for SR and 4.74 mm_3/min for MRR, respectively.

Keywords: Analysis of variance, Gamma coated wire, GRA, Multi-response optimization Nitronic-30

1 Introduction

The manufacturing sector demands high-precision machining techniques as a result of technological advancements. Similarly, intricate component geometries demand highly precise machining. Due to its ability to create complicated shapes, WEDM is the non-traditional machining technique that is most usually employed. Conductive materials can be easily cut with WEDM because there is no mechanical contact between the workpiece material and wire electrodes. The WEDM technique is thus precise and special. Because of its superior machining capabilities, WEDM is used in sectors like the nuclear, automotive, and manufacturing industries. Since the inception of WEDM, research has been ongoing with the goal of enhancing the functionality of WEDM process. Because of the complex and nonlinear character of the WEDM process, a strong correlation between machining parameters and performance traits must be demonstrated.

Wire breakage is a critical and time-consuming concern during the WEDM process. Rethreading is a non-value-adding activity once it has been broken, whereas background activities use a considerable amount of energy. Complex workpiece shapes, energy supply fluctuations, greater peak current values, and wire electrode materials all play a significant role in wire breaking. The effects of wire breakage are reported as higher machining time and poor machined surface quality. The goal of WEDM users right now is to reduce product machining time. The system's main component is the wires utilized in wire electrical discharge machining. Electrodes made of brass wire are a common WEDM tool. However, demand for a wire electrode with performance superior to the traditional brass electrode wire is growing along with the latest diversification in applications of manufacturing fields. It would be reasonable to expect that a coated wire electrode would offer both quick cutting and increased precision.

New materials with progressively greater strengths and capacities are continuously being developed, and response characteristics depend not only on the machining parameters but also on the materials of the work part. Nitronic-30 is nitrogen-strengthened austenitic stainless steel. Its strength to weight ratio is high and therefore may allow lighter gauges to further reduce the costs. It has an ultimate tensile strength of up to 1400 Mpa. It offers excellent fatigue and wear resistance compared to other steels.

*Corresponding author (E-mail: gvpatil@bldeacet.ac.in)

The purpose of the present research work is to use gamma coated wire electrode material to investigate the impact of peak current, pulse on time, pulse off time and servo voltage on output responses and to carry out multi-response optimization of Nitronic-30 material.

1.1 Literature review

The majority of researchers have discovered that increasing the pulse on time and peak current accelerates material removal because they increase the number of electrons that hit the work surface during a single discharge, which removes extra material from the workpiece surface every discharge. Similar to this, given a constant pulse on time and peak current, MRR falls with increased pulse off time and spark gap voltage. Long pulse-off time causes the temperature of workpiece to drop before the next spark ignites, which lowers MRR. High MRR is the result of high discharge frequency, which is caused by high peak current. By facilitating the quick and easy egress of eroded material from the spark gap, increasing wire tension increases MRR. Higher pulse-on times accelerate the degradation of brass wire while also increasing the rate at which metal is removed; the leftover brass wire particle adheres to cutting surface[1-9]. Ashish Goyal[10] found that compared to untreated tool electrodes, MRRimproves using cryogenically treated tool electrodes. This is because a wire material has superior abrasive and mechanical properties provide the process with more energy since increased conductivity encourages more electron emission. According to the physics and mechanism, the bubbles that are created after each pulse on time burst and eject the material off the work surface, producing massive and deep craters. Surface imperfections in these craters lead to an increase in surface roughness. This is explained by the fact that the plasma channel expands as the pulse on time increases.

The majority of researchers have observed the surface roughness increases as pulse on time and peak current increase[1-4,8,11-18]. An average discharge gap widens as a result of increased spark gap set voltage, improving surface precision due to steady machining. The fluctuation of the wire decreases as the wire tension rises, providing the specimens a more dominant surface finish[19]. Unexpectedly, it was found that wire tension, with a value of about 40%, is the most significant factor that considerably affects surface roughness because the cutting width is controlled by the tension applied on the wire. In addition, less undesirable contact in between workpiece and the wire would result in fewer contacts or short circuits, which will improve surface quality. It is commonly known that flushing pressure contributes to a superior surface finish by preventing unwanted contact between particles and the machined surface[12]. Many researchers have found that wire tension and wire feed have less or negligible effect on the materialremoval rate as compared to pulse on-time and pulse- off time[5,8-9,11-12,20-23].

Only a few researchers have used Grey Relational Analysis (GRA) optimize the process parameters[3,6,24-26]. It is necessary to establish a mathematical model in order to accomplish theobjectives of the process. Grey relational analysis is an evaluation technique that uses more factors and fewer data than other statistical approaches to examine the relationship between process parameters and output responses[3]. On the basis of their own presumptions or prior experience, the majority of authors have assigned weights (importance) to the various quality characteristics[3].

Also, the researchers have addressed the issues related with corner error, formation of crater, spark location, properties of dielectric and found that increase in wire tension led to the increase in corner error. As wire tension increases, the wire becomes straighter, which helps in stabilizing the voltage between both the two electrodes. Therefore, there is an increase in heat flux and material disintegration at the corners. The corner deviation increased, leading to additional corner error[16]. According to experimental data, the spark location in WEDM is always asymmetrically scattered along the thickness direction. The usefulness and reliability of components manufactured by WEDM, particularly in the aerospace industry, will suffer as a result of this phenomena. Additionally, the location of the spark is directly related to the machining properties, including cutting efficiency and surface integrity. For the WEDM to perform better, monitoring overall distribution of spark locations and then making improvements to it are essential[8]. Sparks that occur at the conductive phase, causing melting or maybe evaporation, are another contributor to the formation of the craters on the WEDMed surface. It isclear that the rough surface is caused by the large crater diameters[27]. The discharge process is clearly influenced by the characteristics of the dielectric. The

cutting stability can be increased by water-soluble materials' good dispersibility[14].

It is evident from the literature that very few researchers have worked on identifying the causes of wire breakage and their effects. They have suggested ways to avoid the wire breakage. The wire feed should always be set at maximum. This leads to less wire breakage and improved machining stability. Wire breakage and inaccurate work results from improper tension adjustment. (Selvam & Kumar 44) Higher voltages can be applied to thicker workpiece without fear of wire breakage. This is because a thick part allows the power in the wire to be dispersed over a greater area. By increasing the wire speed, wire breakage can reduce. (Saliya 43) Brass wire breaks more frequently as its rate of wear increases with input energy[6].

Axial speed (Wire feed rate) is crucial in preventing localized high temperatures and preventing wire breakage as a result. (Shahane & Pande, 45) When cutting corner shapes, the wire electrode tends to break quickly and the shape precision tends to decline. During the procedure, the wire electrode is exposed to discharging explosive forces, electrostatic forces from the application of open voltage, and hydrodynamic forces from jet flushing. The wire then deflects in the direction that is not parallel to the cutting direction. On the other hand, due to significant debris stagnation in the small, machined kerf, wire breakage is mostly caused by discharge concentrations at the same spot. Therefore, dielectric fluid jet flushing with nozzles has traditionally been used for smooth debris removal. However, a high flow rate may encourage considerable wire vibration and deflection, which degrades shape accuracy and causes wire breaking. (Ebisu, Kawata, Okamoto, Okada, & Kurihara, 11) Though very few studies have been undertaken to avoid wire breakage by using coated wire electrodes and developing new electrode material. (Mohammedazharudeen & Sivasubramanian 29)

The majority of the work has been done on a variety of materials, including Inconel, tool steel, hybrid metal, polycrystalline diamond, and shape memory alloy, to examine the impact of cutting parameters. Brass wire has been used by the majority of researchers.[5-6, 12, 20, 32, 34-40], many have used zinc coated brass wire.[10,11,13-14,17-18,22,41-49], and very few have used molybdenum[23,29,50-54], tungsten wire (Kamei, Okada, & Okamoto 18) and copper wire (Datta & Mahapatra 10) (Hewidy, El-Taweel, & El-Safty 15) as wire electrode to perform the experiments.

The detailed literature review shows that, as current wires don't meet all requirements, more investigation and experimentation are needed to improve cutting efficiency with novel core and coating material combinations. Nowadays zinc-coated brass wires are used which consist (approximately 5 microns) zinc coating on the core. Compared to regular brass wires, this wire significantly increases cutting speed. The problem with the zinc coated wire is that zinc merely coats the surface of the wire core and has a low melting point. The intensity of the spark discharge tends to blast the zinc off the wire core before it has a chance to reach its full potential. So, in order to provide sufficient adhesion to the core wire, the coating must have a high zinc concentration and a higher melting point. High brittleness of gamma phase brass restricts the thickness of the gamma coating to less than 5 microns as thicker coatings will shatter and peel off during the final drawing process. Gamma phase brass is so brittle therefore it actually fractures during the final drawing process, leaving a surface that is somewhat irregular (slightly cracked). This discontinuous surface offers the advantage of speeding up cutting as the wire passes through the cut. Therefore, in the present work an attempt has been made to optimize the process parameters using gamma coated wire electrode material which is novelty of this research work.

It is important to examine the relationship between the input and output parameters as the WEDM is impacted by several factors, which also affects the quality characteristics. Numerous studies have employed the Taguchi and GRA approaches for optimizing the process parameters. A further analysis of the literature reveals that numerous researchers have employed the Taguchi-based GRA approach for multi-response optimization, as well as ANN, RSM, and genetic algorithms. As a result, multi-response optimization can be achieved effectively using the GRA technique.

2 Materials and Methods

2.1 Workpiece material selection

Despite the fact that Nitronic-30 has a lot of potential in applications such as automotive parts, material handling equipment and maritime applications, there is undoubtedly a research gap in the literature regarding usage of this material. Nitronic-30 is nitrogen-strengthened stainless steel developed for applications requiring a good level of aqueous corrosion resistance combined with good toughness. Nitronic -30 Stainless

Steel provides higher yield strength than other types of stainless steel and, therefore, may allow lighter gauges to further reduce costs. Nitronic 30 is difficult to cut using conventional machining as it possesses high hardness. It requires the use of resulfurized lubricant and slow speeds during conventional machining. Also, breakers and curlers are required due to the tough texture of the chips. WEDM is a very good option while machining these types of materials. The workpiece was procured as a rectangular plate with dimensions of 300 mm in length, 300 mm in breadth, and 5 mm in thickness. The chemical composition of Nitronic -30 are mentioned in Table 1. Gamma-coated wire with a 0.25 mm diameter was used as an electrode during experiments on a CNC wire electric discharge machine made by Electronica Supercut 704. The dielectric media used was deionized water.

2.2 Experimental setup

The following figures show a detailed representation of the experimental setup. The experiments were performed on machine of Electronica Supercut 734 on which. It was made sure that the plate was mounted at proper alignment with the bed. Figure 1 shows the Nitronic-30 plate after cutting operation with scale bar.

2.3 Selection of process parameters

The effect of four key control variables, namely pulse on time, pulse off time, peak current, and servo voltage, on material removal rate and surface roughness, has been thoroughly investigated. The control variables mentioned above were chosen after a thorough literature review.[9,11,12,20-23,57]. Furthermore, preliminary trials were carried out prior to the actual experimentation in to establish the parametric levels. During preliminary trials, the phenomenon of wire breakage was intensely studied while selecting parametric levels. Other than control variables, all other parameters were considered as constant variables. Table 2 contains information about the variables and their levels.

2.4 Experiment design using response surface methodology

In the current study, twenty-seven experiments were planned based on the Box Behnken design using in Minitab 17 statistical software, and the input parameters such as pulse on time, pulse off time, peak current, and servo voltage were varied to determine their effects on the responses. To safeguard against noise factor that might fluctuate during the experiment and affect the results, replication and randomization strategies were used. Each experiment was repeated twice and the average of these two readings is considered for calculation of kerf width. Table 3 shows the levels of variables selected for experimentation work.

The Table 4 shows the parametric combination of 27 experiments with different levels.

Table 1 — Chemical composition of Nitronic- 30.

Element	C	Si	Mn	Cr	S	N	Ni	Fe
% Composition	0.005	0.2	15.52	15.90	0.005	0.18	2.9	Balance

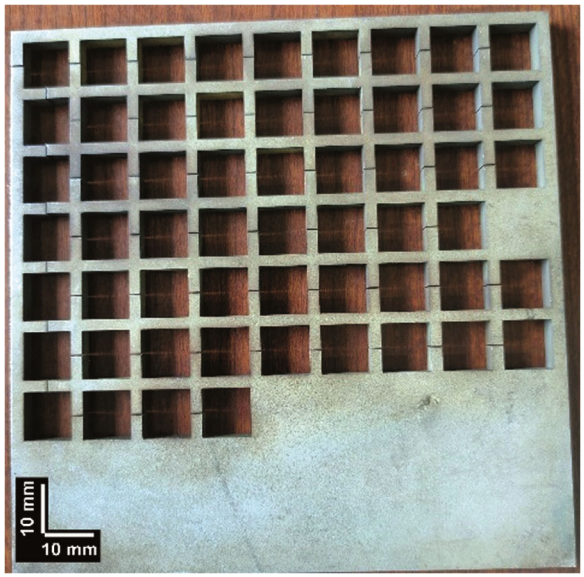

Fig. 1 — Plate after cutting.

Table 2 — List of constant and controlled parameters.

Controlled Variables	Constant Parameters	
Pulse on Time (Ton)	Workpiece material	Nitronic-30
Pulse off Time (Toff)	Workpiece Thickness	5 mm
Peak current (IP)	Wire Electrode	Gamma Coated Brass wire
Servo Voltage (SV)	Servo Feed	2120 mm/min
	Wire Feed	4 Machine Units
	Wire Tension	8 Machine Units

Table 3 — The level of variables chosen for the Box–Behnken design.

Controlled Variable	Coded Variable level		
	Low	Center	High
	-1	0	+1
Pulse on Time (Ton) Machine Units	105	110	115
Pulse on Time (Ton) Machine Units	40	50	60
Peak Current (IP) Amp	70	150	230
Servo Voltage (SV) Volt	20	40	60

2.5 Response variables evaluation

2.5.1 Material removal rate

The term "kerf width" refers to the measurement of a cut slot formed during material removal during machining, whereas "cutting length" refers to the distance an electrode wire travels while machining a workpiece's dimensions. A coordinate measuring device was used to measure the kerf width. Fig. 2 shows the optical profile projector showing the plate mounted on it. The magnified image of the kerf is visible on the screen. The kerf is aligned with the dotted line on the screen and readings are taken by setting the parameters on the digital display.

Due to poor flushing of debris, which causes varied voltage and consequently varying cutting speed, the cutting speed values that were presented on the monitor somewhat deviate from a mean value. Equation (1) is used to compute the material removal rate and the cutting speed is calculated by dividing the cutting length i.e.40 mm by the time taken for cutting the slot. For each machining experiment, three measurements were taken on the machined slot, and the average of these values was used for calculation and analysis.

Table 4 — Parametric combination of factors.

Expt. No	Ton	Toff	IP	SV
1	105	40	150	40
2	115	40	150	40
3	105	60	150	40
4	115	60	150	40
5	110	50	70	20
6	110	50	230	20
7	110	50	70	60
8	110	50	230	60
9	105	50	150	20
10	115	50	150	20
11	105	50	150	60
12	115	50	150	60
13	110	40	70	40
14	110	60	70	40
15	110	40	230	40
16	110	60	230	40
17	105	50	70	40
18	115	50	70	40
19	105	50	230	40
20	115	50	230	40
21	110	40	150	20
22	110	60	150	20
23	110	40	150	60
24	110	60	150	60
25	110	50	150	40
26	110	50	150	40
27	110	50	150	40

The following equation is used in this investigation to calculate MRR.

$$MRR = Kw*Mt*V \quad \ldots (1)$$

Where, Kw = kerf width, Mt= Material thickness, Vc= Cutting speed

2.5.2 Surface roughnes

To calculate surface roughness, a Mitutoyo surface roughness tester is employed. The average arithmetic surface roughness was calculated at three distinct locations, and the result was recorded for study. Fig. 3 shows the surface roughness tester showing Ra value and Fig. 4 shows the graph of the roughness profile.

3 Results and Discussion

3.1 Experimental results

Table 5 shows the experimental results for surface roughness and material removal rate.

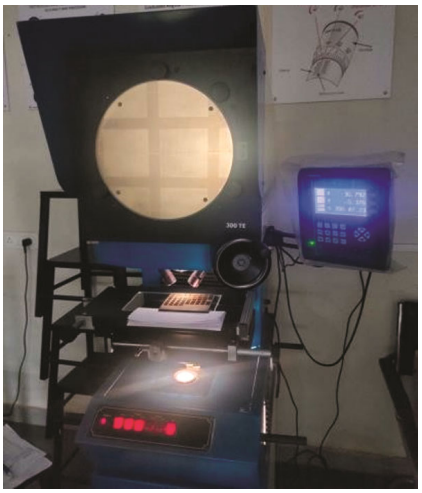

Fig. 2 — Optical profile projector showing the workpiece mounted on bed with magnified kerf.

Fig. 3 — Sample reading.

As shown in Table 6, the results of the ANOVA analysis help in understanding each parameter's influence and contribution to MRR. It can be observed from Table 6 that TON (p-value <0.05) is the most significant parameter influencing MRR with 59.47%. TOFF, IP & SV were found to be insignificant. The R-Square value of the ANOVA models created for the purpose is 91.71%. The main diagnostic method for evaluating the model's suitability is residual analysis. The amount of variation in the response that the model is unable to account for is measured by the residual error. The p-value of 0.1612 is not less than 0.05. Therefore, there is no proof that the model does not effectively account for the response variation. It is also obvious that the process exhibits no outliers and follows a normal distribution. (Fig. 5)

Here, pulse on time (Ton) is regarded as the key influential process parameter that controls the duration of the electric spark generation and consequently has a significant impact on the machining outcomes. The length of time during which electric sparks are produced is called a Ton.

According to the mean effect plot (Fig. 6), an increase in Ton will definitely raise the temperature, expanding the Heat Affected Zone (HAZ) to a larger area. During the Ton, this large HAZ zone of material is flushed away with dielectric fluid, increasing the MRR. The impact

Fig. 4 — Sample graph.

Table 5 — Experiment Results.

Expt. Number	Surface Roughness Ra(micron)	Material Removal Rate (mm^3 /Min.)
1	1.751	2.33
2	3.246	3.65
3	1.662	1.68
4	2.199	3.87
5	2.135	3.29
6	2.239	3.03
7	1.941	2.89
8	1.908	3.38
9	1.743	2.35
10	3.393	3.61
11	1.744	1.74
12	2.072	4.74
13	1.986	3.03
14	1.823	2.32
15	2.128	2.71
16	2.033	2.90
17	1.641	2.08
18	2.305	4.52
19	1.705	2.96
20	3.236	4.90
21	2.029	2.44
22	2.082	2.98
23	2.084	4.58
24	2.031	2.28
25	1.971	4.00
26	1.906	3.63
27	2.022	3.60

Table 6 — ANOVA Results for MRR.

Source	DF	Adj SS	Adj MS	F Value	P-Value
Linear	4	13.4643	3.3661	23.57	0.000
TON	1	12.2875	12.2875	86.06	0.000
TOFF	1	0.6138	0.6138	4.30	0.060
IP	1	0.2553	0.2553	1.79	0.206
SV	1	0.3077	0.3077	2.15	0.168
Square	4	2.1366	0.5342	3.74	0.034
TON* TON	1	0.1374	0.1374	0.96	0.346
TOFF*TOFF	1	2.0503	2.0503	14.36	0.003
IP*IP	1	0.2465	0.2465	1.73	0.213
SV*SV	1	0.4876	0.4876	3.41	0.089
2 Way interaction	6	3.3470	0.5578	3.91	0.021
TON*TOFF	1	0.1893	0.1893	1.33	0.272
TON*IP	1	0.0603	0.0603	0.42	0.528
TON*SV	1	0.7485	0.7485	5.24	0.041
TOFF*IP	1	0.2000	0.2000	1.40	0.260
TOFF*SV	1	2.0071	2.0071	14.06	0.003
IP*SV	1	0.1419	0.1419	0.99	0.338
Error	12	1.7134	0.1428		
Lack of Fit	10	1.6118	0.1612	3.17	0.263
Pure Error	2	0.1016	0.0508		
Total	26	20.6614			

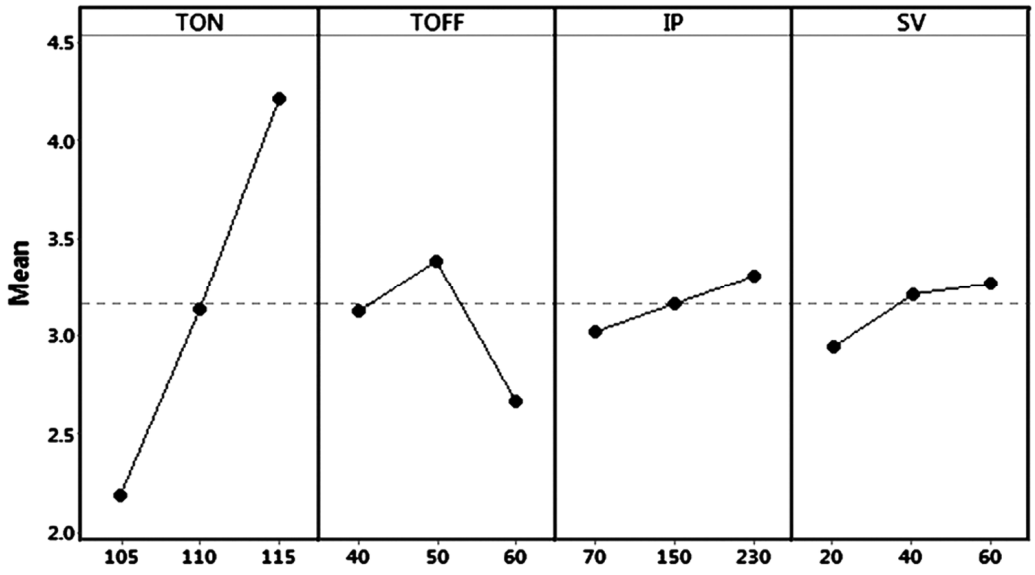

Fig. 5 — Main effect plot for MRR.

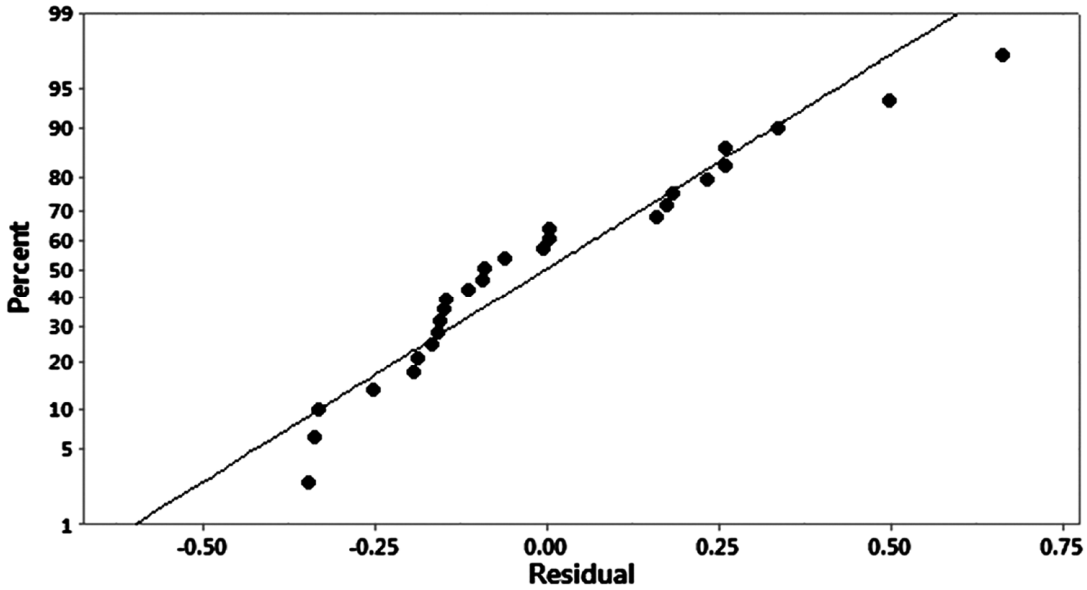

Fig. 6 — Normal probability plot for MRR.

of Toff on MRR is quadratic. The increase in MRR is shown from 40 to 50 but the MRR decreases from 50 to 60. This is attributed to the dielectric fluid motion that results in cooling near the HAZ as the Toff time increases and the material gets solidified again and the debris is not properly flushed out hence leading to reduced MRR. The MRR increases linearly with peak current (IP) due to the fact that as IP increases the current intensity increases which leads to more spark energy leading to more amount of metal to melted and being removed from the workpiece. A higher servo voltage (SV) causes a higher gap voltage, which encourages a higher voltage, more intense spark discharge. Increased MRR at lower servo voltage is mostly caused by a smaller discharge gap. If the gap was too narrow for ionization to occur, the current would flow freely and a high current arc would be visible, increasing the MRR. The greater value of SV denotes that the gap was sufficient for ionization to occur. Additionally, as servo voltage increases, the MRR increases as well.

Figures 7 and 8 depict the relationship between the process parameters. It can be disclosed that MRR reduces with decrease in Ton & increase in Toff due

to the fact that when toff is longer, its cutoffs spark creation and also allows the dielectric fluid to flush. As TON and IP increase, the MRR increases, because the high amount of spark energy will be available for a longer period to remove the excess amount of material from the workpiece. Also, the combination of increments in TON and SV has led to an increase in MRR. The combination of lower Toff and higher SV values has shown a significant effect on MRR. This is because the amount of energy for higher values of SV will be more and as the Toff is low the duration for the time for which the spark is off is less, hence more amount of material will be eroded from the material and hence increase in MRR is observed.

ANOVA shows that TON (p-value <0.05) is the most significant parameter influencing SR with 58.18% followed by SV. TOFF & IP were found to be insignificant. The R-Square value of the ANOVA models devised for the purpose is 90.43%. The main diagnostic method for evaluating the model's suitability is residual analysis. The residual error gauges how much variation in the response the model is unable to account for. The 0.052 P-value cannot be less than 0.05. Therefore, there is no proof that the

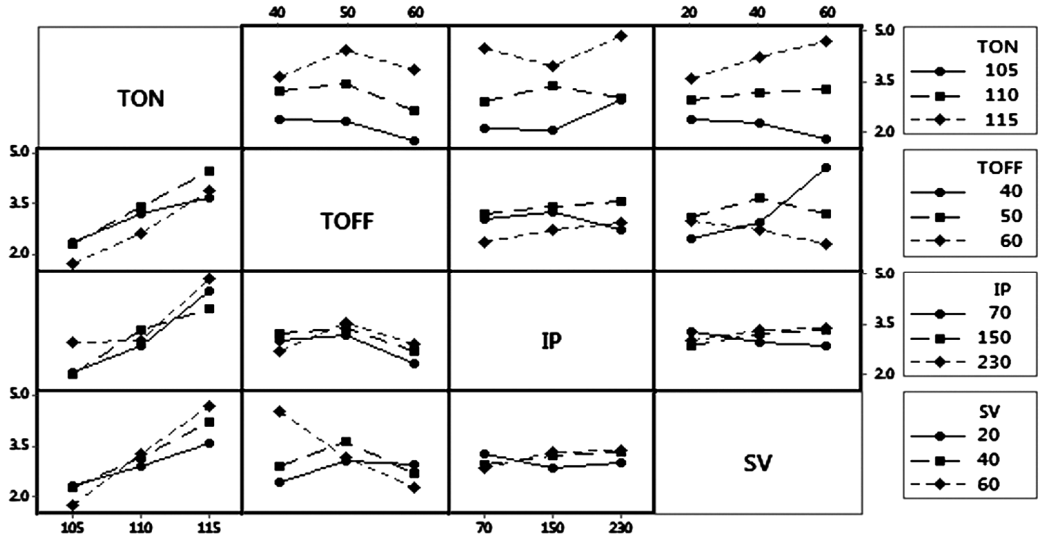

Fig. 7 — Interaction plot for MRR.

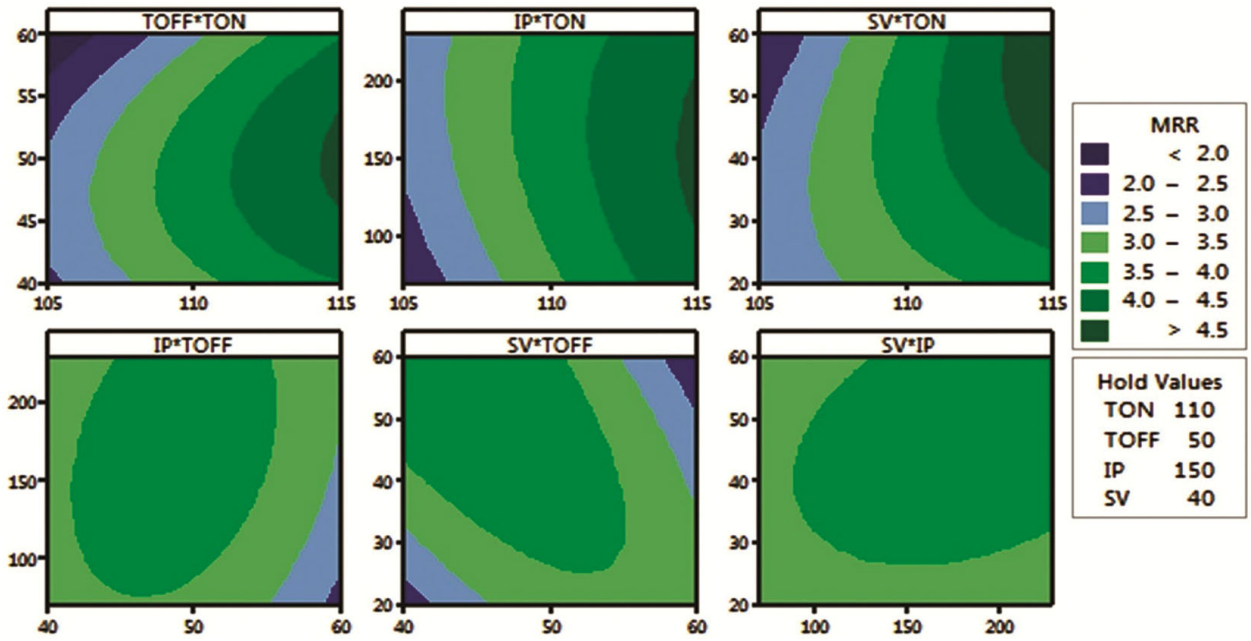

Fig. 8 — Contour plot for MRR.

model does not effectively account for the response variation. It is also obvious that there is no outlier and that the process is following a normal distribution (Fig. 6)

Table 7 demonstrates that the most significant factor influencing surface roughness is pulse-on time. Surface roughness value increases as pulse-on time increases, as shown in Fig. 9.

An increase in pulse duration causes a rise in heat energy, which in turn stimulates enough material to be removed from the workpiece surface. Increased Ton values cause sparks to be produced, which could expand the HAZ. Additionally, during the flushing process, intermittent surfaces are formed, which reduces the surface quality of the machined parts. It has been discovered that the SR lowers as the Toff value increases. Because the machine will be idle during T-OFF, the decrease in Ra value may be caused by a decrease in electric spark production. This result is an increase in flushing time, which may eliminate the microscopic material that is present on the machined work surface and lessen the possibility of confined welding of particles across the machine surface, which would otherwise result in a decrease in Ra value. The dielectric fluid's effectiveness in clearing debris from the work surface with greater Toff value may have been what led to the lower SR values. The surface roughness value rises together with the peak current. This is due to the fact that higher currents create more spark energy, which erodes more material and produces deep, wide craters with a higher surface roughness value. As the SV rises, it is seen that the SR decreases.

Table 7 — ANOVA Results for SR.

Source	DF	Adj SS	Adj MS	F Value	P-Value
Linear	4	3.82044	0.95511	21.73	0.000
TON	1	3.20850	3.20850	73.01	0.000
TOFF	1	0.16194	0.16194	3.68	0.079
IP	1	0.16756	0.16756	3.81	0.075
SV	1	0.28244	0.28244	6.43	0.026
Square	4	0.29684	0.07421	1.69	0.217
TON* TON	1	0.26790	0.26790	6.10	0.030
TOFF*TOFF	1	0.00187	0.00187	0.04	0.840
IP*IP	1	0.00258	0.00258	0.06	0.813
SV*SV	1	0.02058	0.02058	0.47	0.507
2 Way interaction	6	0.86294	0.14382	3.27	0.038
TON*TOFF	1	0.22944	0.22944	5.22	0.041
TON*IP	1	0.18792	0.18792	4.28	0.061
TON*SV	1	0.43692	0.43692	9.94	0.008
TOFF*IP	1	0.00116	0.00116	0.03	0.874
TOFF*SV	1	0.00281	0.00281	0.06	0.805
IP*SV	1				
Error	12	0.52734	0.04394		
Lack of Fit	10	0.52058	0.05206	15.40	0.062
Pure Error	2	0.00676	0.00338		
Total	26	5.50756			

Model Summary

S	R-sq	R-sq (adj)	R-sq (Pred)
0.209630	90.43%	79.25%	45.28%

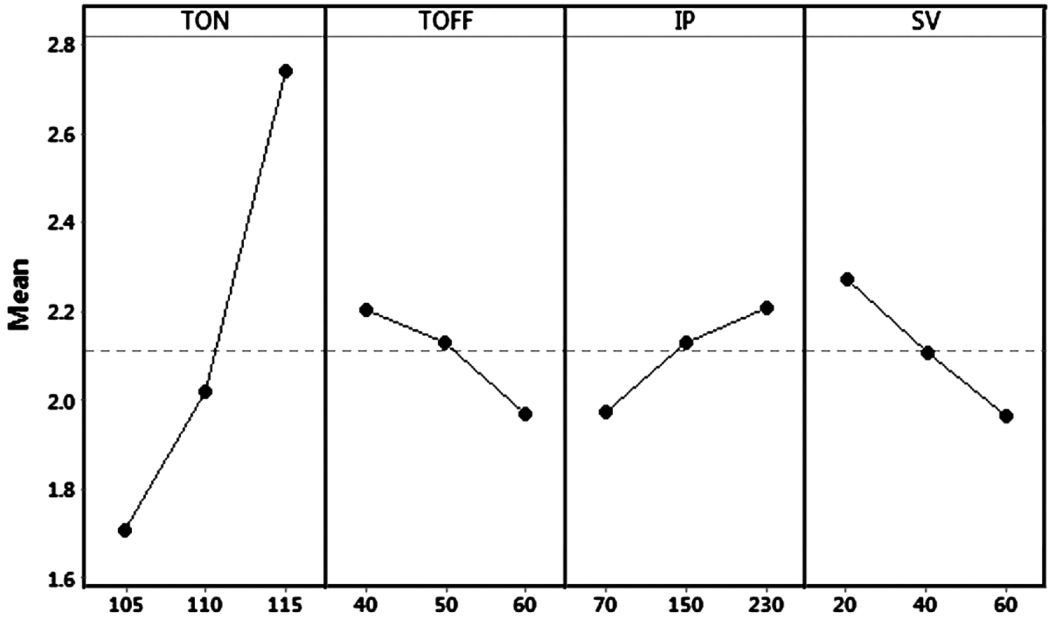

Fig. 9 — Main effects plot for SR.

The interaction plot (Fig. 10) and contour plot (Fig. 11) shows that the combination of highest Ton value with different Toff value has a significant effect on SR. This is because as the TOFF value increases, sufficient time is available to remove the debris from the workpiece and the spark is also off for that period.

The combination of high value of IP with high value of TON shows the depreciation in the surface quality of the workpiece as the excessive amount of spark energy will be eliminating the material at a faster rate. The surface quality not get much affected at other combinations of TON & IP. The combination of reducing TON value and increasing SV value shows very good surface finish quality because as the TON is reduced, the time for which the high amount of spark energy is produced will be less and hence, there will be less amount of wear & tear of the surface. Other combinations such as Toff & IP, Toff & SV, IP & SV don't show that much effect on the SR value.

3.2 Surface morphology analysis

After WEDM processes, machined surface defects were examined using a scanning electron microscope (SEM). SEM images of the surface machined using the WEDM process are shown in Figs (12-15). In order to achieve great surface quality, it is essential to control different process parameters. Higher values of pulse-on time and current result in a higher discharge energy level due to an increase in spark intensity. This leads to formation of globules, craters, microcracks, voids and other surface defects. However, a higher value of pulse-off time provides more time for debris removal with low discharge energy level and reduces the severity of surface defects. The surface

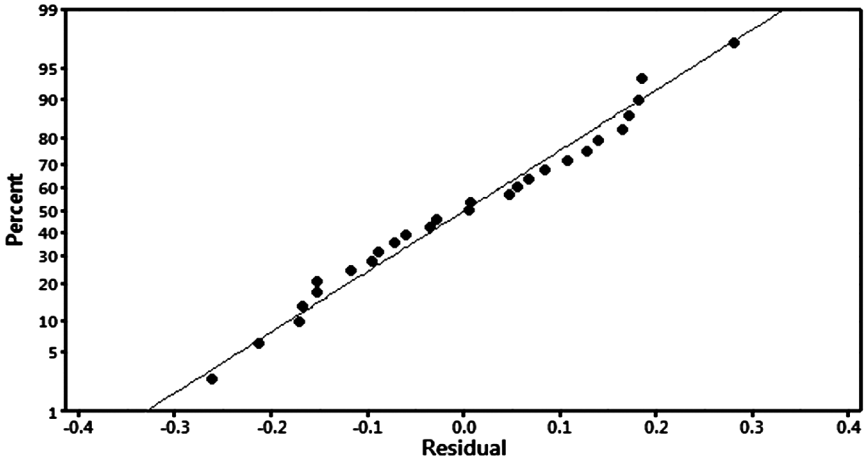

Fig. 10 — Normal probability plot for SR.

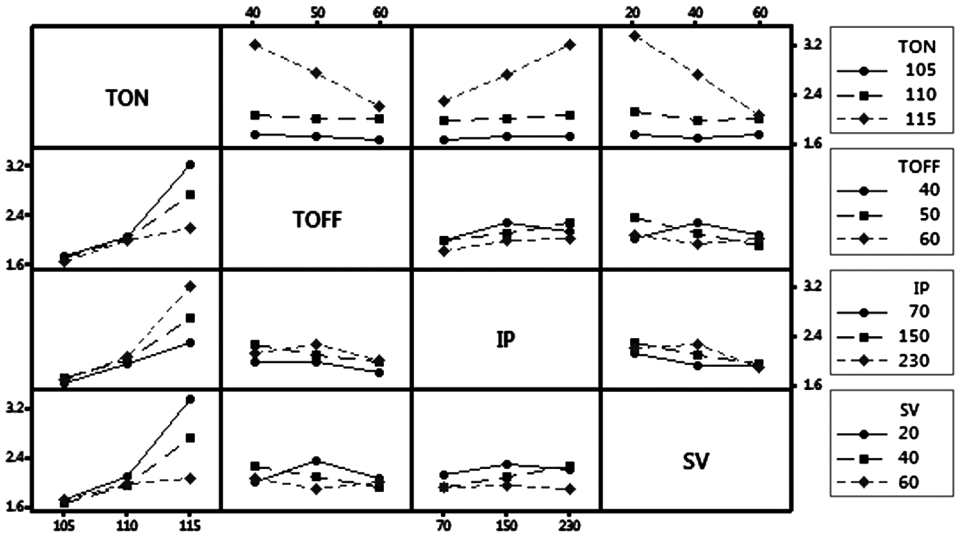

Fig. 11 — Interaction plot for SR.

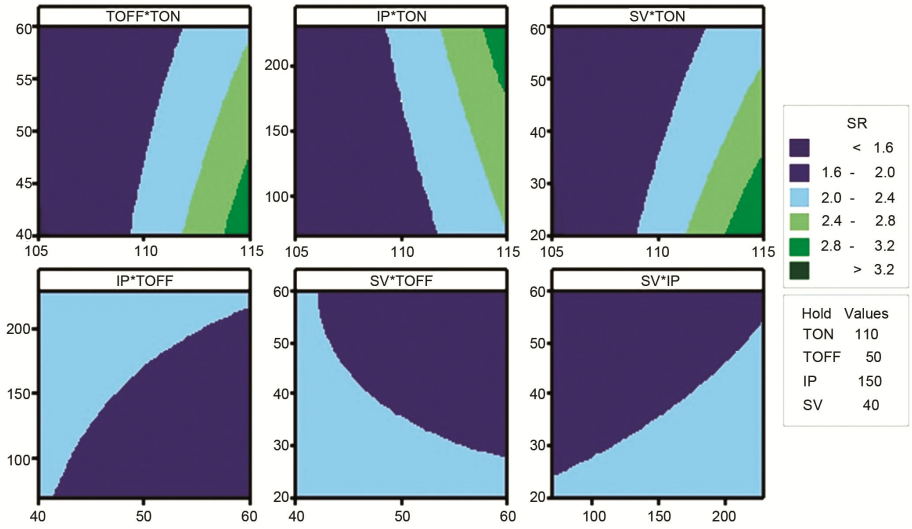

Fig. 12 — Contour plot for SR.

morphology of the machined surface at low and high discharge energies was studied. WEDM process parameter settings for high discharge energy were Ton (115 MU), Toff (50 MU), IP (230 A) & SV (40 V), whereas parameters for low discharge energy were Ton (105 MU), Toff (50 MU), IP (70 A) & SV (40 V).

Figures 13 and 14 show the SEM micrograph of the machined surface at low and high discharge energy levels, respectively. At high discharge energy level with increased pulse on time (115 MU) and current (230A), the severe melting of the work piece takes place. More amount of material gets removed from the workpiece. Due to this excess material removal, some of the debris particles stick in the working zone and get redeposited on the machined surface. This large amount of discharge energy removes large craters from the machined surface and forms the sub-surface. This ensures increased MRR but surface quality gets affected. It is quite evident from the Fig. 14 that large amount of molten material is redeposited on the machined surface. Also, large size globules are formed on the surface leading to poor surface quality. Whereas at lower discharge energy level as shown in Fig. 13, pulse on time (105 MU) & current (70A), the material removal takes place at slower rate. The small size of redeposited molten material is observed. Also, the size of globules is reduced. The narrow craters were observed indicating lower material removal rate. This ensures improves surface quality of the machined sample. However, the complete removal of surface defects is not possible as there will be some amount of discharge at all times at any parameter setting.

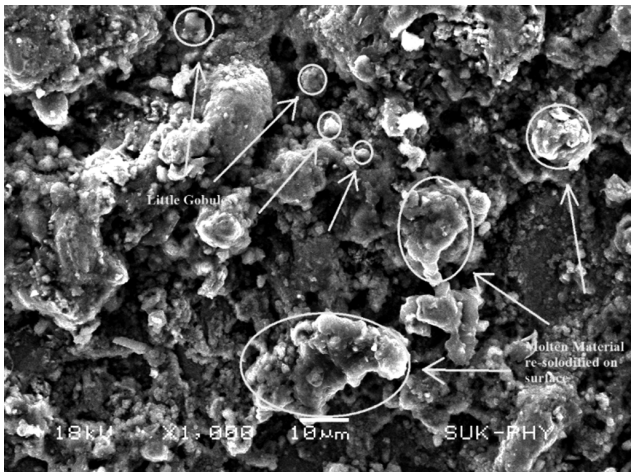

Fig. 13 — SEM image to show little globules and molten material redeposited at lower energy levels.

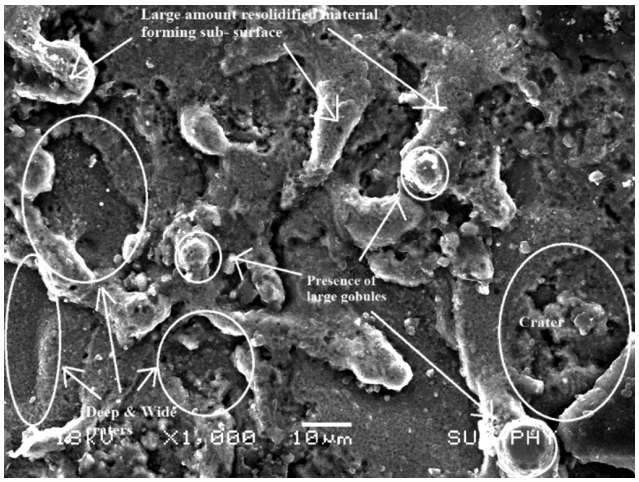

Fig. 14 — SEM image to highlight large globules, deep & wide craters and molten material redeposited at higher energy levels.

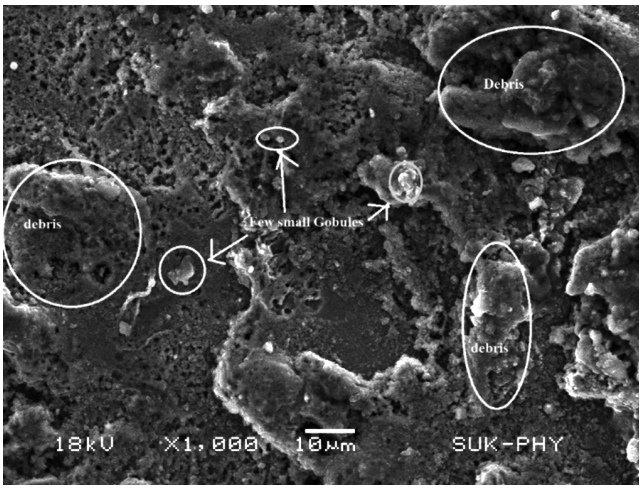

Fig. 15 — SEM image to highlight moderate debris formation and globules at optimized condition.

To achieve higher MRR, pulse on time and current should be set at higher levels and to achieve lower SR pulse on time and current should be set at lower levels. This conflicting situation can be avoided by using multi response optimization. Figure 16 shows the SEM micrograph of the surface machined under optimized parameter settings. The process parameters at optimized conditions are Ton (115 MU), Toff (50 MU), IP (150 A) & SV (60 V). The current rating at 70A shows that the process exhibits the energy level which is not too high or too low. Little presence of globules can be observed on the surface. Also, a moderate amount of molten material redeposited on the surface can be seen. At optimized condition better MRR is observed without affecting the surface quality too much.

3.3 Development of mathematical model

Regression analysis has been used in a mathematical model (Eqs. (2) and (3)) to forecast the output data based on the relationship between the input and output data, with R-square values for MRR and Ra of 91.71% and 90.43%, respectively.

MRR = -79.5 + 1.27 Ton + 0.219 Toff + 0.0270 IP - 0.248 SV - 0.00642 Ton*Ton - 0.00620 TOFF*TOFF - 0.000034 IP*IP - 0.000756 SV*SV + 0.00435 Ton*Toff - 0.000307 Ton*IP + 0.00433 Ton*SV + 0.000279 Toff*IP - 0.003542 Toff*SV + 0.000118 IP*SV ... (2)

SR = 68.3 - 1.578 Ton + 0.499 Toff - 0.0594 IP + 0.353 SV + 0.00897 Ton*Ton + 0.000187 Toff*Toff + 0.000003 IP*IP + 0.000155 SV*SV - 0.00479 Ton*Toff + 0.000542 Ton*IP - 0.00331 Ton*SV + 0.000021 Toff*IP - 0.000133 Toff*SV - 0.000021 IP*SV ... (3)

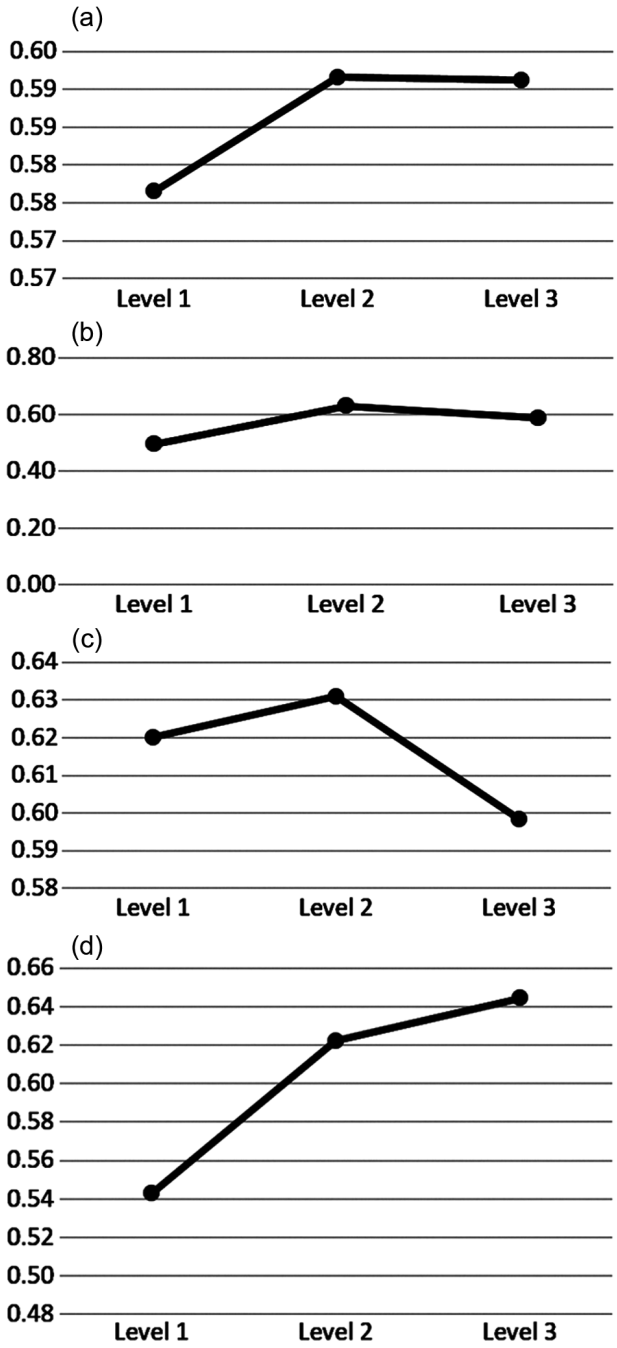

Fig. 16 — Grey relational grade plots for Ton, Toff, IP & SV.

3.4 Multi-response optimization by GRA method

Due to their inherent ability to evaluate various options according to various criteria in order to perhaps determine the best, multi-criteria decision-making (MCDM) procedures are becoming more and more important for complicated and real-world challenges. The popular multi-objective optimization technique known as RSM coupled GRA was used in

this work primarily to accelerate the process of identifying the key influencing parameter and to comprehend the combined impact of input parameters. A grey relational analysis is carried out using the steps listed below.

3.5 Weight calculation using entropy method

Entropy measures the degree of chaos and randomness in the data. Three types of weighting techniques—subjective, objective, and integrated—are defined. The subjective way of weighting the answer variable relies on the decision- maker, who must do so based on his prior experience or level of subject matter expertise. In contrast, the decision maker would have no influence on how the weights are determined in the objective technique. C.E. Shanon's mathematical theory is used to determine the weights.

The weights are determined in this work using an objective method, and the steps are described below.

Step1: Following the normalization of the performance indices, project outcomes are calculated.

$$P_{ij} = \frac{x_{ij}}{\sum_{i=1}^{m} x_{ij}} \quad \text{... (4)}$$

Step2: Entropy measure Calculation

$$E_j = -k \sum_{i=1}^{m} P_{ij} * \ln P_{ij} \quad \text{... (5)}$$

Where, $k = \frac{1}{\ln(m)}$

Step 3: Objective weight Calculation

$$W_j = \frac{1-E_j}{\sum_{j=1}^{n} (1-E_j)} \quad \text{... (6)}$$

In this study, multi-response analysis based on GRA was used to achieve the highest MRR and lowest Ra from the chosen control parameters. Here, MRR and Ra output responses were normalized using larger is better criteria for material removal rate and smaller is better criteria for surface roughness, respectively. Table 8 shows the obtained relevant data, where the trial with the highest GRG value is selected as the best combination of control factor to get a superior output response. Table 8 shows that trial 12 has the greatest GRG values compared to the other combinational control factors. Response means, as shown in Table 8, might be used to obtain the ideal parametric condition for superior output responses. In this hypothetical research, higher levels for pulse on time (Ton), Servo voltage (SV), and medium levels for pulse off time (Toff), peak current (IP), are considered to be the optimal levels. Based on GRA, the maximum value of the GRG is considered to be the ideal parameter. This could also be supported by mean effect plot of the GRG shown in Fig. 13.

GRA provides an effective solution to the uncertainty in multi-input and discrete data problems for multi-response optimization through the selection of machining parameters. According to Table 8, the experiment number 12 has the highest ranking. The related response parameters are SR (2.072 μm), and MRR (4.74 mm^3/min). The experiment number 10 has the lowest ranking with corresponding output responses as SR (3.39 μm), and MRR (3.61 mm^3/min) Table 9, 10 and Fig. 16 shows the ideal level for each parameter is represented by its highest GRG. The highest value of GRG for a particular setting will give the optimized output responses. For Ton, the level 3 (115 MU) provides optimized output response values. It means that the better MRR & SR values are obtained. At higher values of Ton, the high amount of spark energy is available for a longer period to remove the excess amount of material from the workpiece. Therefore, higher MRR values can be observed at this level. Similarly, workpiece surface also gets affected

Table 8 — Grey relation response.

Expt. No.	GR MRR	GR RA	GRG	Rank
1	0.449	0.848	0.648	10
2	0.626	0.276	0.451	26
3	0.394	0.967	0.68	5
4	0.67	0.524	0.597	16
5	0.565	0.554	0.56	20
6	0.528	0.506	0.517	25
7	0.51	0.671	0.591	17
8	0.579	0.697	0.638	12
9	0.451	0.857	0.654	9
10	0.619	0.259	0.439	27
11	0.398	0.856	0.627	13
12	0.929	0.587	0.758	1
13	0.528	0.64	0.584	18
14	0.448	0.771	0.61	15
15	0.489	0.557	0.523	24
16	0.511	0.61	0.561	19
17	0.426	1	0.713	3
18	0.846	0.48	0.663	7
19	0.519	0.905	0.712	4
20	1	0.278	0.639	11
21	0.46	0.612	0.536	22
22	0.522	0.582	0.552	21
23	0.867	0.581	0.724	2
24	0.444	0.611	0.528	23
25	0.699	0.65	0.675	6
26	0.622	0.698	0.66	8
27	0.617	0.617	0.617	14

Table 9 — Response table for GRG means.

	Level 1	Level 2	Level 3	Delta	Rank
TON	0.58	0.59	0.59	0.015	4
TOFF	0.50	0.63	0.59	0.136	3
IP	0.62	0.63	0.60	0.033	2
SV	0.54	0.62	0.64	0.101	1

Table 10 — GRG Improvement with Optimized Parameters.

Setting level	Optimum process parametercombination	
	Predicted	Experimental
	A3B2C2D3	A3B2C2D3
MRR	4.33	4.74
SR	2.30	2.072
GRG	0.5503	0.7581

Enhancement in grey relational grade= 37.76 %

due to abrasive erosion and leads to somewhat poor surface quality which is unavoidable. For Toff, level 2 (50MU) gives the optimized setting. MRR increases from 40 to 50 but it decreases from 50 to 60 because the dielectric fluid motion results in cooling near the HAZ as the Toff time increases and the material gets solidified again and the debris is not properly flushed out hence leads to reduced MRR. For IP, level 2 (150A) considered as optimum level. As the current increases the cutting rate is increased. As IP increases from 150 A to 230 A, the current intensity increases tremendously which leads to more spark energy melting more amount of metal and being removed from the workpiece. But at the same time, it produces deep, wide craters with a higher surface roughness value which leads to poor surface quality. For SV, level 3 (60 V) gives the optimized setting. As servo voltage (SV) increases it causes a higher gap voltage, which encourages a more intense spark discharge which leads to increased MRR. The SR values found to be decreasing as SV increases. The recorded optimal parameters are Ton3, Toff2, IP2, and SV3. For optimum settings, the relevant values are Ton 115 (MU), Toff 50 (MU), IP 150 (A), and SV 60. (V).

3.6 Confirmation test

After selecting the most suitable machining parameters, the analysis is validated using the confirmation test. the optimal machining parameters given by the grey relational analysis are as follows,

$$\gamma = \gamma_m + \Sigma (\gamma_n - \gamma_m) \quad \ldots (7)$$

where,

γ_m = Total mean grey relational grade
γ_n =The mean grey relational grade at optimum level

4 Conclusion

Experimental research has been done to determine the effect of the process parameters on the MRR and Ra of Nitronic-30. A multi-objective optimization technique (RSM coupled GRA) was employed to select the control parameters in order to achieve higher MRR value and lower surface roughness value. The following conclusions are drawn from this paper.

a. Ton is the major variable influencing both MRR and SR with 59.47 % and 58.18% contribution respectively.
b. With increase in Ton and SV, the MRR tends to increase.
c. As Toff decreases, the surface quality gets better.
d. Utilizing the RSM-grey relational grade values, the optimal level of the input process parameters is identified. As a result, it was discovered that the process parameters of Ton 115 (MU), Toff 50 (MU), IP 150 (A), and SV 60 (V) produced the desired outcomes.
e. Experiment No. 12 with highest GRG grade of 0.758 yields optimum results for MRR (4.74 mm^3/min.) & SR (2.072 μm)
f. Within the experimental region, the proposed mathematical model demonstrated great prediction accuracy of 91.71% and 90.43% for MRR &SR respectively.
g. Improvement of 37.36 % is observed in GRG.
h. SEM has revealed that, the size of craters and material re-deposition on machined surface increases with increase in pulse on time and current.

References

1 Bobbili R, Madhu V & Gogia A K, *Eng Science Tech, an Int J, 18* (2015) 664.
2 Cao C, Zhang X, Zha X & Dong C *Procedia Eng, 81* (2014) 1945.
3 Chalisgaonkar R & Kumar J *Engg.Sience and Tech, An Int J, 18* (2015)125.
4 Chaudhari R, Vora J J, Patel V, Lacalle L L & Parikh D M *Materials, 13*, (2020) 4943.
5 Chaudhary T, Siddiquee A N & Chanda A K *Defence Tech, 15*, (2019) 541.
6 Chen S, Xu K, Chang W, Wang Y & Wu Y *Entropy, 24*, (2022) 1796.
7 Chen Z, Moverare J, Peng R L & Johansson S *ProcediaCIRP, 45*, (2016) 307.
8 Chen Z, Zhou H, Yan Z, Han F & Yan H *Mater Res Tech, 13*, (2021) 184.
9 Dabade U A & Karidkar S S *Procedia CIRP, 41* (2016) 886.
10 Goyal A, Rahman H U & Ghani S A *J King Saud University-Eng Sci, 33* (2021) 129.

11 Datta S, & Mahapatra S *Int J Eng Sci Tech, 2* (2010) 162.
12 Ebisu T, Kawata A, Okamoto Y, Okada A & Kurihara H *Procedia CIRP, 68* (2018) 104.
13 Galindo-Fernandez M, Diver C & Leahy W *Procedia CIRP, 42* (2016) 297.
14 He C, *Procedia CIRP, 42* (2016) 591.
15 Hewidy M S, El-Taweel T A & El-Safty M F, *J Mater Processing Tech, 169* (2005) 328.
16 Ishfaq K, Zahoor S, Khan S A, Rehman M, Alfaify A & Anwar S, *Eng Sci Tech, an Int J, 24* (2021) 1027.
17 Jarin S, Saleh T, Rana M, Muthalif A G & Ali M Y, *Procedia, 184* (2017) 171.
18 Kamei T, Okada A & Okamoto Y, *Procedia CIRP, 42*, (2016) 596.
19 Sudhakara D, & Prasanthi G *Procedia Eng, 97* (2014) 1565.
20 Karidkar S S, & Dabade U A *ASME Int Mech Eng Congress Exposition*, *50527*, (2016) p. V002T02A022
21 KASHID D V (2014) *Int J Mech Prod Eng Res Development*
22 Kausar F, Kumar S, Azam M, Suman S, Sharma A,& Sethi A, *J Mech Civil Eng, 12* (2015) 101.
23 Kolli M, Basha S K, Midatana N K, Bedhapudi M & Desina S S, *Int J Mech Eng Tech, 8* (2017) 446.
24 Kumar A, Kumar V & Kumar J, *Adv Mater Sci Eng,* 1 (2013) 1.
25 Kumar S, Dhanabalan S & Narayanan C S, *SN Appl Sci, 1* (2019) 1.
26 Lakshmikanth G, Murali N, Arunkumar G & Santhanakrishnan S, *Int J Scientific Res Develop, 1 (9)* (2013) 1772.
27 Liu J F, Li L & Guo Y B, *Procedia CIRP, 13* (2014) 137.
28 Selvam M P & Kumar P R, *Mech Mech Eng, 21* (2017) 37.
29 Saliya J, *Int J Eng Dev Res, 2* (2014) 3671.
30 Shahane S & Pande S S, *Procedia Mfg, 5* (2016) 205.
31 Lodhi B K & Agarwal S, *Procedia CIRP, 14* (2014) 194.
32 Manoj I V, Soni H, Narendranath S, Mashinini P M & Kara F, *Adv Mater Sci Eng, 1 (2022) 1.*
33 Mohammedazharudeen J & Sivasubramanian R, *Int J Eng Res, 3* (2014) 1.
34 Mori A, Kunieda M & Abe K, *Procedia CIRP, 42* (2016) 601.
35 Naresh C, Bose P S & Rao C S, *SN Appl Sci, 2* (2020) 1.
36 Natarajan K, *J Nanomaterials,1 (2022) 6765721*
37 Prasad L, Upreti M, Yadav A, Patel R V, Kumar V & Kumar A, *SN Appl Sci, 2* (2020) 1.
38 Priyadarshini M, Biswas C K, & Behera A, *Mater Mfg Processes, 34* (2019) 1316.
39 Raj A, Misra J P, Khanduja D, Saxena K K & Malik V, *Int J Interactive Des Mfg* , 1 (2022) 1.
40 Rajesh R, Anand M D & Benny K N, *Int J Mech Eng Tech, 8* (2017) 924.
41 Raju K, *Nanomaterials, 1 (2022) 2903385*
42 Ranganath B, Sudhakar K, Shrikantappa A, *Int Conf on Mech Eng, 1* (2003) 1
43 Rao P S, Ramji K & Satyanarayana B, *Alexandria Eng, 55*, (2016) 1077.
44 Rath D, Chandra P, Kumar S, *Adv Mater Sci Eng, 1 (202) 63 1 6799*
45 Ravi R R, Rachit S H & Mandal A, *Indian J Sci Tech, 9* (2016) 34.
46 Saedon J B, Jaafar N, Yahaya M A, Saad N & Kasim M S, *Procedia Technol, 15* (2014) 832.
47 Shahane S, & Pande S S *Procedia Mfg, 5*, (2016) 205.
48 Sharma N, Khanna R & Gupta R, *Procedia Eng, 64* (2013) 710.
49 Sharma N, Khanna R & Gupta R D, *Eng Sci Tech, An Int J, 18* (2015) 171.
50 Sharma N, Singh A, Sharma R *Procedia Engg., 97*, (2014) 1609.
51 Sharma V S, Sharma N, Singh G, Gupta M K, & Singh G *Materials, 16*, (2023) 114
52 Singh P, Chaudhary A K, Singh T, & Rana A K *Int Research J Engg and Tech, 2*, (2015) 1753.
53 Sivasankar S, & Jeyapaul R *Procedia engg, 38*, (2012) 3977.
54 Takale A M, & Chougule N K *Mater Science and Engg: C, 97*, (2019). 264.
55 Yadav A K, *Int Conf Recent Devop. In Engg*. 1(2017) 252
56 Zaman U K *Materials, 15*, (2022) 7846.
57 Zhu Y, Liang T, Gu L, & Zhao W *Procedia Mfg, 5*, (2016) 849.